

Visual Monitoring and Servoing of a Cutting Blade during Telerobotic Satellite Servicing

Amama Mahmood, Balazs P. Vagvolgyi, Will Pryor, Louis L. Whitcomb, Peter Kazanzides, Simon Leonard

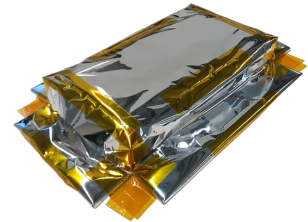
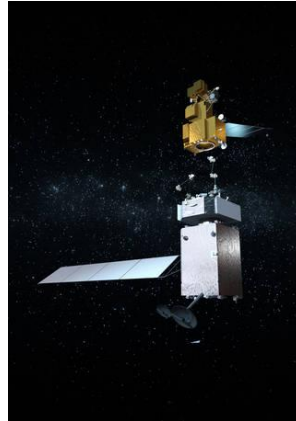
Abstract—We propose a system for visually monitoring and servoing the cutting of a multi-layer insulation (MLI) blanket that covers the envelope of satellites and spacecraft. The main contributions of this paper are: 1) to propose a model for relating visual features describing the engagement depth of the blade to the force exerted on the MLI blanket by the cutting tool, 2) a blade design and algorithm to reliably detect the engagement depth of the blade inside the MLI, and 3) a servoing mechanism to achieve the desired applied force by monitoring the engagement depth. We present results that validate these contributions by comparing forces estimated from visual feedback to measured forces at the blade. We also demonstrate the robustness of the blade design and vision processing under challenging conditions.

I. INTRODUCTION

Ongoing developments in actuation and sensing make the deployment of robot systems in extreme and remote environments the preferred solution over human presence. Because of time delays, which can range from several seconds to minutes, space exploration is among the areas with the greatest need for technologies providing reliable tele-operation. These time delays render direct tele-operation of simple tasks very challenging and lengthy. Although predictive rendering based on 3D and image models can alleviate these challenges, they still rely on a human-in-the-loop to process delayed feedback, which exposes the vulnerabilities to unexpected changes. These unknowns are even more prevalent when a robot interacts with non-rigid or deformable bodies. In this paper, we present a method for remotely monitoring the cutting (whether tele-operated or automated) of the multi-layer insulation (MLI) that covers the envelope of satellite. We propose a physical model for cutting an MLI box by estimating the force applied on its sides by a cutting blade and the engagement depth of the blade from visual feedback. Also, we present an image-based method for servoing the applied force for cutting the box.

The Exploration and In-Space Services (ExIS) Division of NASA launched the Robotic Refueling Mission 3 (RRM3) [1] and announced OSAM-1 [2] (formerly, Restore-L) with the objective to develop the technologies necessary for refueling satellites by robots in space. In particular, OSAM-1 will use Landsat 7 as a test (Figure 1a). On this satellite, the fuel ports are covered by a non-rigid MLI box (or “hat”), which must be cut on three sides to access the ports. This delicate procedure, in close proximity of the satellite envelope, will be performed by a robot equipped with a circular blade at the altitude of 680km. It will involve time delays between four

Authors are with the Laboratory for Computational Sensing and Robotics (LCSR) at Johns Hopkins University, Baltimore USA



(a) Artist rendering of OSAM-1 servicer (bottom) approaching Landsat-7 (top). Image courtesy of NASA.

(b) Replica of MLI box covering fuel ports on Landsat-7.

Fig. 1: The OSAM-1 mission aims to refuel the Landsat-7 satellite. One critical task of the mission will be to cut an MLI box (1b) that covers the fuel ports on three of its four sides.

and seven seconds because of multiple up-down links (earth to satellite and reverse) and the signal buffering delays which occur at each device interface [3]. To facilitate the monitoring and execution, we propose to use images from the on-board cameras to monitor locally and servo the execution of the cut.

The main contributions of this paper are threefold. First, we propose a physical model between the side of an MLI box and the blade by a pulley interacting with a string attached to coiled springs at both ends. Second, as the circular blade cuts through a side, the force exerted by the blade deforms the MLI and we present a method for estimating the applied force by visually measuring the engagement depth of the blade in the MLI. Finally, by relating the engagement depth of the blade to the applied force, we formulate a control law to adjust the force applied to the MLI, during teleoperation, to ensure a uniform cut along a side.

II. PREVIOUS WORK

We previously reported the results of a study where trained NASA robot operators operated our ground-based system to cut two sides of the MLI box under a software-imposed time delay of 5 seconds [4]. These experiments evaluated the effectiveness of various visualization and control interfaces, based on subjective operator feedback and objective measures such as task completion time and completeness of

cutting (i.e., number of MLI layers cut). While MLI cutting success rates ranged between 90% and 100%, depending on the configuration, it was often difficult to maintain the desired engagement of the cutting blade due to the time delay between the actual deformation of the MLI and the visualization of that deformation. This delay also affects visualization of, and reaction to, cutting failures. For example, a time consuming task is to reengage the blade in the cutting path after being accidentally pulled out or, conversely, pulling the blade from under the MLI after being pushed in too deep. These observations led to the measurement and control strategies reported in this work.

A surprisingly similar problem to visually estimating forces during MLI cutting is found during micromanipulation of cells and, in particular, for the penetration of embryos with micropipette. Examples of these methods can be found in [5], [6] and visual features similar to the ones proposed in our research are used to model deformations and estimate the force applied on the surfaces. Other prior work in the visual estimation of applied force includes the application of neural networks to estimate forces during minimally-invasive surgery [7], [8]. In the area of robotically assisted surgeries, several haptic methods are based on measuring deformation from camera images to estimate applied forces and render them to a human operator [9], [10]. These aforementioned methods, however, require advanced computer vision methods such as stereo vision, optical flow, deformable meshes and depth maps. None of these technologies is suitable for the limited onboard computational resources nor are they suitable for the challenging reflections caused by the MLI.

Complementary to rendering forces, several methods are proposed to model deformable bodies by interacting or poking at them [11], [12]. A review of a related method is presented in [13] and a classification of models is proposed based on the level of elasticity and mesh of the material.

Finally, the control of interaction between a robot and a deformable model has been investigated in several areas. In particular, visual servoing is used to follow straight lines for a welding application [14], to follow a contour during electrocautery of tissues [15] and to manipulate deformable volumes [16]. Each of these image-based visual servoing methods proposes a different interaction matrix to control the motion of the robot by minimizing error of an image-based command. Our research takes the same approach by proposing a novel image-feature that captures the engagement depth of a circular blade in an MLI blanket.

III. METHOD

To understand the dynamics of cutting the MLI blanket, we propose a model that estimates the applied force on the MLI from visual feedback. Given the lack of reliable force sensing near the blade for OSAM-1, it is imperative to maintain a steady force of the tool against the deformable surface. We propose to use visual feedback to assess this force since cameras are available to the operators. The goal of this section is to propose a model that measures MLI surface deformation to determine the applied force by the

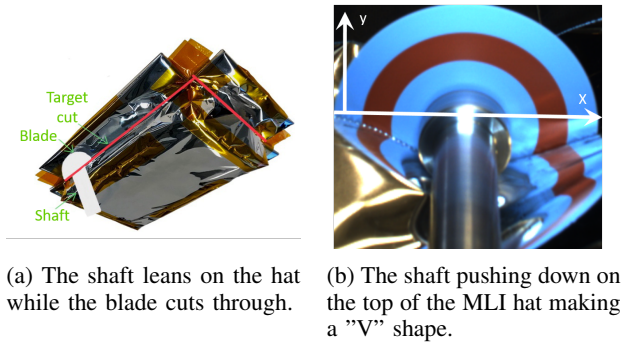


Fig. 2: Interaction of blade assembly with the MLI hat.

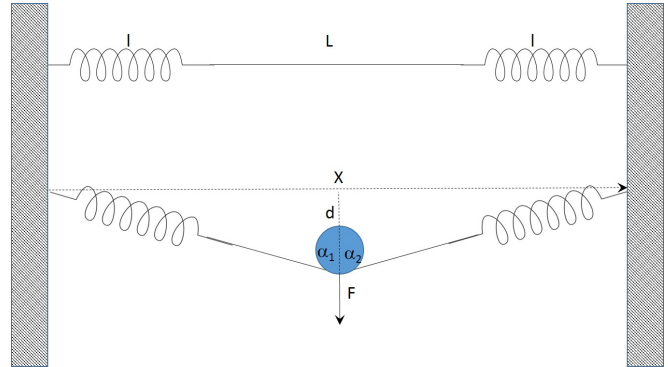


Fig. 3: Model used to estimate applied forces by measured angle.

tool. Although the blade applies little force to the MLI, the shaft that holds the blade applies the bulk of the force (albeit a small one) as it pushes on the top of the surface to make sure that the blade cuts through all the layers of the hat. Fig. 2a shows how the shaft leans on top of the hat during the cutting process.

This force can be observed visually as the MLI passes under the shaft as seen in Fig. 2b and the more the shaft pushes down, the more a “V” shape is observed on each side. The proposed model aims to understand the relationship between the “V” angle that can be visually observed and the force applied by the tool. A similar dynamic between a tool and a deformable body is observed for microinjection of a single cell, where the surface of the cell deforms similarly under the force applied by a pipette [17].

A. Model

Let the model illustrated in Fig. 3 represent the surface of the MLI by a string of length L . Each corner of the MLI box is maintained by a coil spring of length l such that the total length of the system at rest, including springs, is $T = L + 2l$. A pulley on top of the string has horizontal coordinate x and is pulled down with a vertical displacement d until a force F is obtained. Let α_1 and α_2 be the angles of each side of the pulley. In this section, we introduce a model between α_1 , α_2 and F to obtain a function $F = f(\alpha_1, \alpha_2)$.

First, we note that $\alpha_1 = \arctan(\frac{x}{d})$ and $\alpha_2 = \arctan(\frac{2l+L-x}{d})$ and the length of each hypotenuse is $h_1 = d/\cos(\alpha_1)$ and $h_2 = d/\cos(\alpha_2)$. At the position (x, d)

of the pulley, the overall length of the string and springs is $h_1 + h_2$ and length difference with the system at rest is $\Delta T = h_1 + h_2 - L - 2l$. At equilibrium, each spring is stretched by $\Delta T/2$ and using Hooke's law each spring applies a force $F_1 = F_2 = K\Delta T/2$, where K is the spring constant. The vertical components of F_1 and F_2 are $f_{1y} = F_1 \cos(\alpha_1)$ and $f_{2y} = F_2 \cos(\alpha_2)$ with $F = f_{1y} + f_{2y}$.

The relationship between the angles α_1 and α_2 and F is non-linear and also depends on the vertical coordinate of the pulley d . Although d is not known during a cutting operation, its value affects the values of α_1 and α_2 at a given x and can be used to achieve a desired F^* .

B. Vision-Based Force Sensing

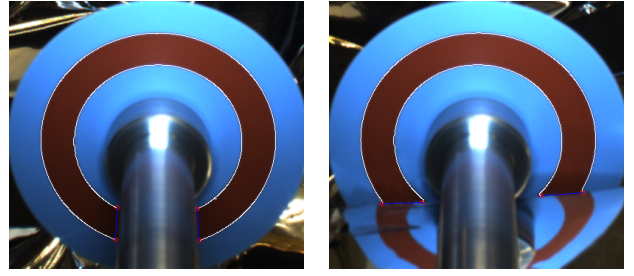
To estimate the force applied by the blade on the MLI according to the model of Section III-A, the angle described by the MLI around the blade must be measured, as illustrated in Fig. 4b. The outer cover of an MLI blanket has a metallic reflective film (kapton or aluminium) which makes usage of standard computer vision algorithms extremely challenging for detecting MLI occlusion [18]. As an example, Fig. 4a shows a typical image obtained without MLI occlusion, whereas Fig. 4b shows the blade during cutting with MLI occlusion and the reflections of the blade on the outer layer. Although occlusion adds to the challenges of using vision-based force detection, the algorithm stays fairly consistent for MLI hats as there is little to no variability in materials according to the guidelines presented by NASA [19]. Beyond the MLI blanket, the hat assembly is specific to Landsat-7.

To compute the angle robustly, we use concentric circles with colors that offer a sharp contrast in a color space. In our implementation, we selected the HSV color space and use the red and cyan colors of the H (hue) channel. These colors are 180° apart on the hue channel which ranges between 0 and 360° . Canny edges are extracted from the hue channel and the result is masked with predefined templates of two thin rings where the transition between colors is expected. The expected result is a long edge on each side of the red circle from which the endpoints are found, as illustrated in Fig. 4b. These endpoints represent the coordinates where the MLI occludes the blade by altering the expected hue pattern. By fitting a line through each pair of endpoints on both sides of the shaft, the angles α_1 and α_2 described by the MLI are computed. Typical results are presented in Fig. 4.

We note that if K and d are unknown, the force estimated from α_1 and α_2 will be recovered up to an unknown scale factor Kd . We consider that the estimation of K , either online or offline, to be a separate research problem. For this research, the value of K was approximated offline from experimental data.

C. Visual Servoing

Section III-A introduced the relationship between the angles described by the MLI on each side of the blade and the applied force on the MLI. The driving parameter to achieve a desired force $F^* = f_{1y}^* + f_{2y}^*$ at a given point x is the depth of the blade d . Thus, given the corresponding desired angle



(a) Blade without MLI occlusion. (b) Blade with MLI occlusion.

Fig. 4: Masked Canny edges (white) with endpoints (red circles) and fitted lines (blue lines).

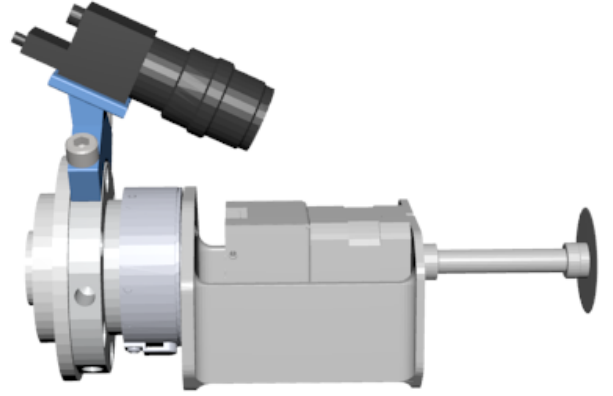


Fig. 5: Assembly model of the force sensor, camera, motor and blade.

$\alpha^* = [\alpha_1^* \ \alpha_2^*]^T$, the objective is to minimize $\mathbf{e} = \alpha - \alpha^*$ which is achieved by the differential equations $\dot{\alpha} = L\dot{d}$ where $L\dot{d}$ is the time derivative of $[\tan(\frac{x}{d}) \ \tan(\frac{2l+L-x}{d})]^T$ which gives

$$L = \begin{bmatrix} \sec^2(\frac{x}{d})\frac{x}{d^2} \\ \sec^2(\frac{2l+L-x}{d})\frac{2l+L-x}{d^2} \end{bmatrix}. \quad (1)$$

IV. EXPERIMENTS

We tested our models by cutting MLI blankets with a UR-10 robot (Universal Robot, Odense, Denmark) equipped with a force/torque sensor and a DC motor (Anaheim Automation, Anaheim, CA). The shaft of the motor is terminated with a 45mm rotary cutter blade spinning at 4,000 RPM. A 1920×1080 RGB camera (FLIR, Wilsonville, OR) is mounted above the motor looking down at the blade and forming approximately a 400×350 region of interest. The lens of the camera is also equipped with a LED ring light for consistent light conditions. A 3D model of the fully assembled tool is illustrated in Fig. 5. Sheets of MLI blankets were pinned on a soft EPS foam frame. The blankets are composed of 14 alternating layers of tulle and polyester film (McMaster-Carr 8567K102) between two external layers of metalized PET film (CS Hyde, Lake Villa, IL).

A. Blade Engagement Depth

The algorithm of Section III-B is used to measure angles described by the MLI against the blade in the background.

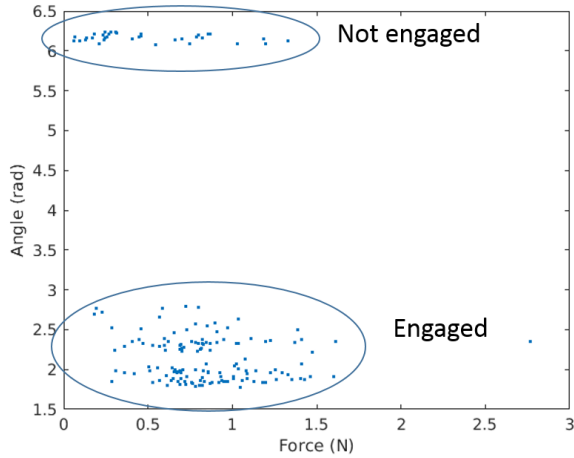


Fig. 6: Scatter plot of measured forces (magnitude) versus measured angles.

Plain MLI blankets were pinned on top of a “U” bracket made out of soft foam such that the cutting area is suspended between two compliant uprights. The UR-10 had the blade initially above the MLI and was manually jogged downward to pierce the MLI and then jogged horizontally to cut the blanket. Meanwhile, the endpoints and resulting occlusion lines of the MLI were computed at each frame and compared to points that are manually selected. The average pixel error for each endpoint was 6.2 with a standard deviation of 5.1.

One of the most common large sources of error is due to the MLI reflecting light sources on the blade. These reflections cause the colors on the blade to saturate and prevent the edge detector from detecting the rings on the blade.

1) *Force Detection and Estimation:* The objectives of these experiments are to determine the magnitude of the forces applied by the tool on the MLI and to validate if the slopes of the MLI that are visually observed can be used to detect and estimate these forces. The setup of Section IV-A was used for manually cutting the MLI between two points. During the cut, forces/torques were recorded from the sensor as well as the angle $\alpha = \alpha_1 + \alpha_2$ described by the MLI around the tool.

a) *Visual Force Detection:* Fig. 6 illustrates the scatter plot of the data points collected in two groups. The first group corresponds to when the blade was above the MLI and the measured forces are mainly a result of noise and the robot is moving downward (the average measured force magnitude was 0.35N). Correspondingly, the measured angle α corresponds to approximately 2π . A typical image of this case is presented in Fig. 4a.

The second group corresponds to when the blade was engaged in the MLI at various depths. The first observation is that forces during cutting have an average magnitude of 0.85N. The second observation is that both visual and force measurements can tell these two groups apart (t-test $p < 0.001$).

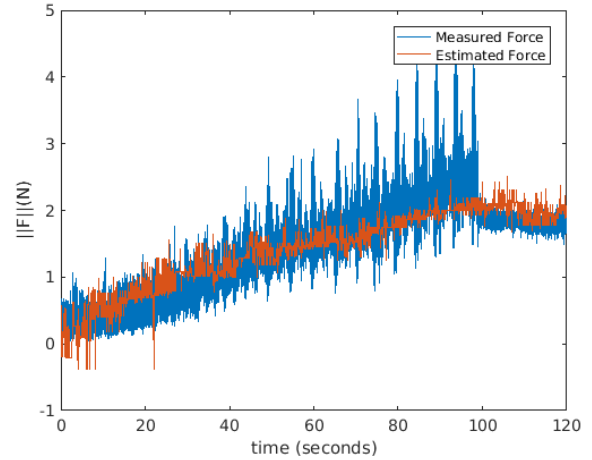


Fig. 7: Measured force from the force sensor compared to the force estimated from the model at $L/2$. The depth of the blade was obtained from the UR-10 kinematics and the angles α_1 and α_2 from measurements.

b) *Visual Force Estimation:* In this set of experiments, the objective is to validate the model of Section III-A. The first experiment validates the effect that the depth d has on the applied force and measured angles at a given x coordinate (fixed x and varying d). The experiment starts with the blade in the middle of the MLI blanket ($x = L/2$) with the blade halfway inserted in the MLI but without applying any force. Then, the blade is pushed deeper and data is collected to compare the measured forces to the estimated ones provided by the model. The true depth of the blade (as provided by kinematics) and the measured angles α_1 and α_2 are used to estimate the force. The procedure is repeated at $x = L/4$ and $x = 3L/4$. The effect of the depth on the applied force is illustrated in Fig. 7, where the forces computed by the model are compared to the measured ones. The root mean squared (RMS) error between the measured forces and force estimates is 0.3293N. Similarly, Fig. 8 shows the effect of the depth on the measured angles and $\alpha_1 + \alpha_2$ and the RMS error between the measured angles and angle estimates is 4.1597° .

B. Visual Servoing

The last experiment demonstrates the usage of a vision-based control law to adjust the depth of the blade to achieve desired MLI angles α_1^* and α_2^* and consequently F^* . As with Section IV-A.1.b, we are interested in validating the control law in two scenarios: the first one with a constant x and the second one with a varying x .

In the first experiment, the blade is inserted at $x = L/2$ and $d = 0$ and the commanded angles are set to $\alpha_1^* = \alpha_2^* = 1.25\text{rad}$. The procedure is also repeated at $x = L/4$ and $x = 3L/4$ with $\alpha_1^* = 1$ and $\alpha_2^* = 1.5$ radians. In all cases, the experiments were repeated when the angles were initially greater than their expected values (blade moving down and increasing forces) and when the angles were smaller (blade

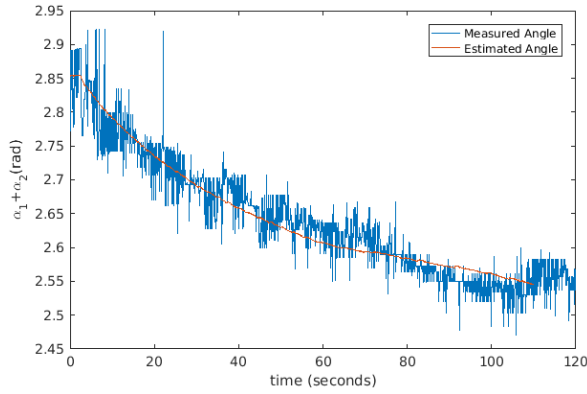


Fig. 8: Measured $\alpha_1 + \alpha_2$ compared to the estimated sum at $L/2$. The depth of the blade was obtained from the UR-10 kinematics.

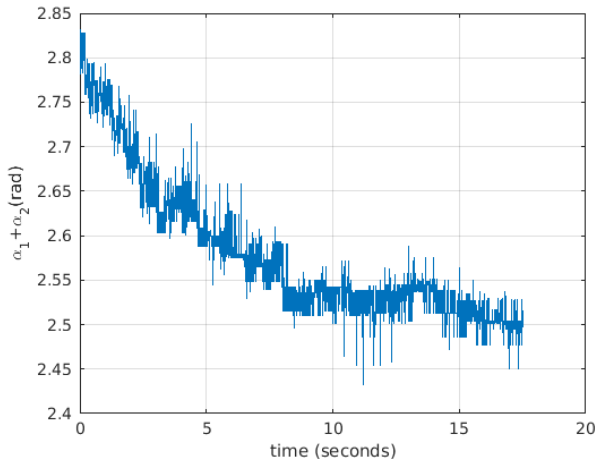


Fig. 9: Visual servoing to achieve $\alpha_1 + \alpha_2 = 2.5$ at $L/2$. The blade had an initial depth measured by $\alpha_1 + \alpha_2 = 2.8$ radians and the visual servoing lowered the blade to achieve $\alpha_1 + \alpha_2 = 2.5$.

moving up and decreasing force). The resulting trajectories for $\alpha_1 + \alpha_2 = 2.5$ at $L/2$ are illustrated in Fig. 10 and Fig. 9. Both figures demonstrate the convergence of the system at $\alpha_1 + \alpha_2 = 2.5$. The velocity of the blade was limited to 1 mm/s to mitigate the effects of occasional outliers for α_1 and α_2 (see the large spike in Fig. 10 for an example). Note the large spike in the measured angles caused by a glare on the blade. Although these artifacts do happen occasionally and do affect the force estimation, their effects on velocity and stability are limited by the small velocity limit that the UR-10 can move the blade.

Finally, visual servoing is used to control the depth of the blade during an MLI cut. A trajectory of α_1^* and α_2^* is generated at each horizontal coordinate $x(t)$ to achieve the desired force F^* . Then, the blade is inserted at $x(0) = 0$ with a depth $d = 0$. The servoing is used to push the blade down until $\alpha_1 + \alpha_2 = 2.2$ radians, which took approximately 290 seconds. This combination of α_1 and α_2 was determined experimentally to provide a force of 2 N at

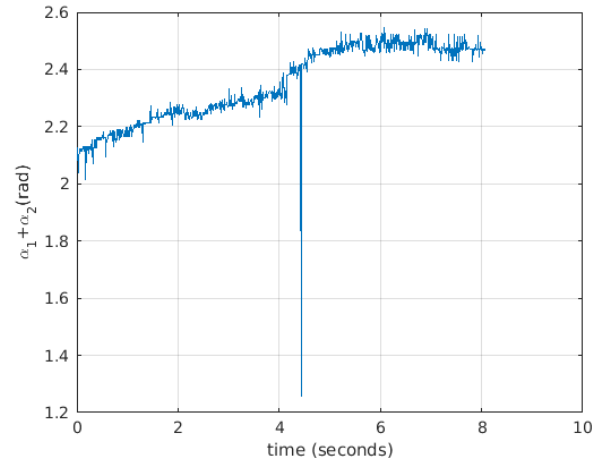


Fig. 10: Visual servoing to achieve $\alpha_1 + \alpha_2 = 2.5$ at $L/2$. The blade had an initial depth measured by $\alpha_1 + \alpha_2 = 2.1$ radians and the visual servoing raised the blade to achieve $\alpha_1 + \alpha_2 = 2.5$.

$x = 0$. Then, a constant velocity of 1mm/s is applied along the cutting direction to move the blade horizontally while the control law of Section III-C is used to control the vertical velocity. The trajectory of $\alpha_1 + \alpha_2$ was computed to reach 2.5 radians at $L/2$ to also obtain force of 2 N. The resulting trajectory in Fig. 11 shows the measured $\alpha_1 + \alpha_2$ along with the corresponding command, while the plot in Fig. 12 shows the measured force magnitude with the corresponding desired force magnitude. In both cases, we note that the desired commands are achieved, although the measured force appears to be consistently smaller than the desired one. One possible explanation for this is the possible misalignment of the cutting direction with the blade's plane or the top layer of the MLI that slightly peels off during the cut and increases the α_1 and α_2 without increasing force applied to the MLI.

V. CONCLUSION AND DISCUSSION

This paper introduces a novel model for using visual feedback for monitoring and servoing the cutting of a non-rigid material. The model relates the visual features extracted from images of the task to the force applied by the cutting tool. The visual features used in this paper are the angles described by the material being cut as it passes under the shaft of the blade. We propose a method for measuring these angles in a challenging environment involving specular material by designing a circular color pattern to facilitate the detection of the blade as it cuts through the material. Finally, the engagement depth of the blade is controlled with a visual servoing control law to ensure that a constant desired force is applied throughout the cut. In future work, we plan to address the problem of cutting MLI with a weaker structure, such as when one or two sides of the MLI box are already cut and only two sides of the box remain.

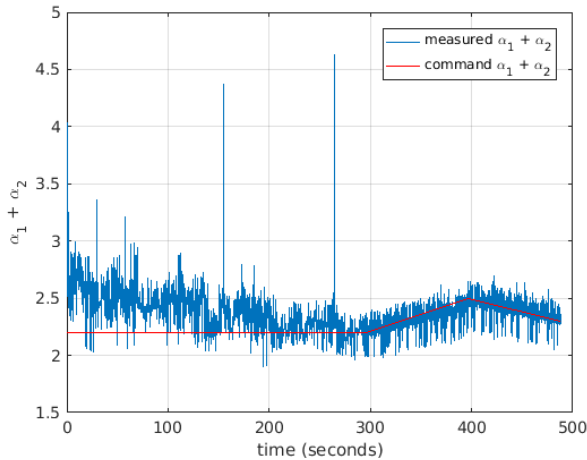


Fig. 11: Servoing of a trajectory during a horizontal cut. The blade was inserted autonomously until the desired angles α_1 and α_2 were measured. The blade was moved horizontally to cut through the MLI. The trajectory of α_1 and α_2 was precomputed to maintain a force of 2 N by using known α_i values at $x = 0$ and $x = L/2$ and interpolated linearly between these two points.

ACKNOWLEDGMENTS

This work is supported by NASA NNG15CR66C. We thank Brian Roberts, Billy Gallagher and the ExIS team at NASA GSFC. Anton Deguet assisted with the software and system integration of the experimental platform. Adarsh Malapaka assisted with mechanical design of the tool and configuration of the system.

REFERENCES

- [1] NASA GSFC, "Robotic Refueling Mission." [Online]. Available: <https://sspd.gsfc.nasa.gov/RRM3.html>
- [2] —, "On-Orbit Servicing, Assembly and Manufacturing 1 Mission." [Online]. Available: <https://nexis.gsfc.nasa.gov/OSAM-1.html>
- [3] T. B. Sheridan, "Space teleoperation through time delay: Review and prognosis," *IEEE Transactions on robotics and Automation*, vol. 9, no. 5, pp. 592–606, 1993.
- [4] W. Pryor, B. P. Vagvolgyi, W. J. Gallagher, A. Deguet, S. Leonard, L. L. Whitcomb, and P. Kazanzides, "Experimental evaluation of teleoperation interfaces for cutting of satellite insulation," in *IEEE Intl. Conf. on Robotics and Automation (ICRA)*, May 2019, pp. 4775–4781.
- [5] J. Kim, F. Janabi-Sharifi, and J. Kim, "A haptic interaction method using visual information and physically based modeling," *IEEE/ASME Transactions on Mechatronics*, vol. 15, no. 4, pp. 636–645, Aug 2010.
- [6] F. Karimirad, S. Chauhan, and B. Shirinzadeh, "Vision-based force measurement using neural networks for biological cell microinjection," *Journal of Biomechanics*, vol. 47, no. 5, pp. 1157 – 1163, 2014. [Online]. Available: <http://www.sciencedirect.com/science/article/pii/S0021929013006283>
- [7] A. I. Aviles, S. M. Alsaleh, J. K. Hahn, and A. Casals, "Towards retrieving force feedback in robotic-assisted surgery: A supervised neuro-recurrent-vision approach," *IEEE Transactions on Haptics*, vol. 10, no. 3, pp. 431–443, 2016.
- [8] C. Gao, X. Liu, M. Peven, M. Unberath, and A. Reiter, "Learning to see forces: Surgical force prediction with RGB-point cloud temporal convolutional networks," in *MICCAI Workshop on Computer Assisted and Robotic Endoscopy (CARE)*, Sept. 2018, pp. 118–127.
- [9] W. Kim, S. Seung, H. Choi, S. Park, S. Y. Ko, and J. Park, "Image-based force estimation of deformable tissue using depth map for single-port surgical robot," in *2012 12th International Conference on Control, Automation and Systems*, Oct 2012, pp. 1716–1719.

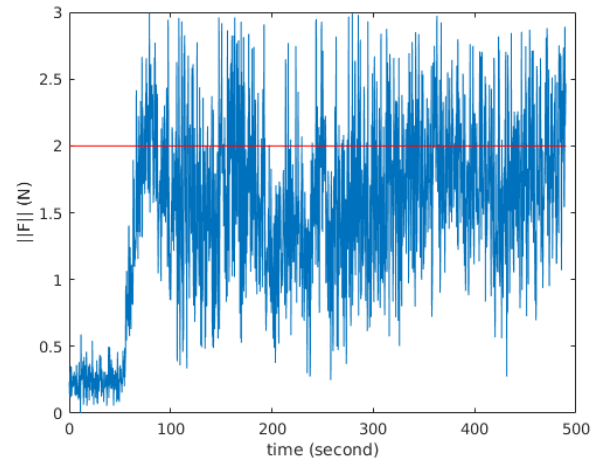


Fig. 12: Measured force at the blade compared to the desired 2 N command. The actual cutting trajectory started at 290 seconds and moved the blade at 1 mm/s. Contact with the MLI is around 50 seconds. The increase in noise is caused by a combination of sensor noise, interaction between the MLI and the blade and the servoed motion of the robot.

- [10] E. Noohi, S. Parastegari, and M. efran, "Using monocular images to estimate interaction forces during minimally invasive surgery," in *2014 IEEE/RSJ International Conference on Intelligent Robots and Systems*, Sep. 2014, pp. 4297–4302.
- [11] P. Boonvisut and M. C. avuolu, "Estimation of soft tissue mechanical parameters from robotic manipulation data," *IEEE/ASME Transactions on Mechatronics*, vol. 18, no. 5, pp. 1602–1611, Oct 2013.
- [12] M. A. Greminger and B. J. Nelson, "Modeling elastic objects with neural networks for vision-based force measurement," in *Proceedings 2003 IEEE/RSJ International Conference on Intelligent Robots and Systems (IROS 2003) (Cat. No.03CH37453)*, vol. 2, Oct 2003, pp. 1278–1283 vol.2.
- [13] J. Sanchez, J.-A. Corrales, B.-C. Bouzgarrou, and Y. Mezouar, "Robotic manipulation and sensing of deformable objects in domestic and industrial applications: a survey," *The International Journal of Robotics Research*, vol. 37, no. 7, pp. 688–716, 2018.
- [14] N. Andreff, B. Espiau, and R. Horaud, "Visual servoing from lines," *The International Journal of Robotics Research*, vol. 21, no. 8, pp. 679–699, 2002.
- [15] J. D. Opfermann, S. Leonard, R. S. Decker, N. A. Uebele, C. E. Bayne, A. S. Joshi, and A. Krieger, "Semi-autonomous electrosurgery for tumor resection using a multi-degree of freedom electrosurgical tool and visual servoing," in *2017 IEEE/RSJ International Conference on Intelligent Robots and Systems (IROS)*, Sep. 2017, pp. 3653–3660.
- [16] D. Navarro-Alarcn, Y. Liu, J. G. Romero, and P. Li, "Model-free visually servoed deformation control of elastic objects by robot manipulators," *IEEE Transactions on Robotics*, vol. 29, no. 6, pp. 1457–1468, Dec 2013.
- [17] S. Permana, E. Grant, G. M. Walker, and J. A. Yoder, "A review of automated microinjection systems for single cells in the embryogenesis stage," *IEEE/ASME Transactions on Mechatronics*, vol. 21, no. 5, pp. 2391–2404, Oct 2016.
- [18] A. Artusi, F. Banterle, and D. Chetverikov, "A survey of specular removal methods," in *Computer Graphics Forum*, vol. 30, no. 8. Wiley Online Library, 2011, pp. 2208–2230.
- [19] M. Finckenor and D. Dooling, "Multilayer insulation material guidelines," 1999.